Journal of Energy Engineering and Thermodynamics
ISSN: 2815-0945
Vol: 02, No. 05, Aug-Sep 2022
http://journal.hmjournals.com/index.php/JEET
DOI: https://doi.org/10.55529/jeet.25.1.19

Modelling of Four-Port Converter for Electric Vehicle Applications

S.Sharma[1*], K.Rajambal[2], C.Kalaivani[3]

[1,2,3]Department of EEE, Puducherry Technological University*

Email: [2]rajambalk@pec.edu, [3]kalaivani46@pec.edu
Corresponding Email: [1]sharma.sha@pec.edu*

Received: 29 May 2022 **Accepted:** 13 August 2022 **Published:** 15 September 2022

Abstract: Multiport Converters (MPC) combine various renewable power sources through a single-stage power conversion. They offer the benefits of centralized control, excellent reliability, easy circuit configuration, small packaging, and cheap manufacturing cost & size. Due to its great efficiency and dependability, using a Multiport Converter to include renewable energy & energy storage into the bipolar dc bus is a preferable alternative. Full-bridge interleaving bidirectional buck/boost semi active rectifier with bi-polar output converter, a typical four-port converter (FPC), is specifically and in-depth examined in terms of operation principles, voltage and power relationship, port current ripples, soft switching performance, & control. The modelling and simulation studies of the FPC for PV, battery, and bipolar outputs in MATLAB/Simulink suggested in this paper. Effects of duty ratio at different battery voltage and battery charging and discharging at various duty ratio verified. The power flow analysis done for different intensities of PV and Battery voltage and load conditions.

Keywords: Multiport Converter, Electric Vehicle, DC – DC Converter, PV and Battery

1. INTRODUCTION

The popularity of DC distribution networks is rising. Because of improvements in power electronic technology and the expansion of sectors with dc loads, like as data centres and battery electric automobiles, electric vehicles (EVs) will eventually overtake other modes of transportation as the preferred choice [1]. Modern DC systems may do considerably more complex tasks than only voltage regulation. As a result, they are gaining popularity as a solution for a variety of domestic and commercial applications, including DC-powered residences, quick EV charging places, hybrid energy storage systems (ESS), & renewable energy parks.

Different types of renewable energy sources (RESs), such as PV, wind and geothermal, are the promising clean energy sources for the future. Due to the unpredictability of these RES,

Journal of Energy Engineering and Thermodynamics
ISSN: 2815-0945
Vol: 02, No. 05, Aug-Sep 2022
http://journal.hmjournals.com/index.php/JEET
DOI: https://doi.org/10.55529/jeet.25.1.19

ESS, like batteries & super capacitors, have been frequently deployed in conjunction with renewable energy sources. Energy storage enables generation sources to operate at maximum efficiency while accommodating variations in demand without the need to ramp up or down. As a result, system stability and power quality can be guaranteed. To control power fluctuations and reduce electricity costs, the RESs' redundant energy may be stored in the ESS [2]. Lithium-ion batteries have drawn a lot of attention recently since they are an energy storage solution that has both high energy density and long-lasting.

Onboard energy storage systems have received a lot of attention lately due to a rise in interest in the applications that make use of them, such as electric automobiles, electrified railway vehicles, electric ships, electric boats, and electric aircrafts [3]. Batteries, ultracapacitors, fuel cells, flywheels, or a combination of them, can serve as the foundation for these energy storage systems.

The two main categories of EV charging station architectures are common ac bus and common dc bus. The latter appears to be preferable because it requires fewer conversion stages to achieve a greater system efficiency and makes it simpler to integrate storage systems (batteries or ultra-capacitors) RES. Using three-level neutral-point-clamped (NPC) converters, the conventional dc-bus design can be implemented as bipolar dc bus systems [4]. One of the greatest popular is the bi-polar DC Bus system. 2 wires, one with +ve polarity and the other with -ve polarity, make up a bi-polar DC bus. The current through ground is 0 in normal operation. With the right management measures, a metallic return is also conceivable. The following benefits of this topology outweigh its greater technical complications, expense, and dependability over the unipolar DC: During normal process, the current via the return wire is lower, which reduces power losses; if a fault develops on one bus, the operation of the other buses is unaffected and continues to be normal [5]-[6]. By charging and discharging the corresponding capacitors, the balancing circuit would preserve the voltages on the positive and negative poles. Given that the current drawn is decreased, this is advantageous when certain loads require a lot of electricity. When transferring the same amount of power, the current flowing in a bipolar dc network can be cut in half compared to the one in a unipolar network [7]-[10]. The aim of this paper is to influence the efficiency boundaries of the multi-port converter-based EV charging station.

A multiport converter is preferable to numerous single-input converters in a freestanding renewable energy system because it has the advantages of a simpler circuit, higher efficiency, and cheaper cost. Multiple input and/or output ports on multi-port converters allow for the connection of power supplies and electric loads. The converter regulates the flow of electrical energy between power sources and loads. Every port has the ability to transfer energy in both directions [11]-[15]. An MPC acts as a single power converter and it connects a number of elements at different port. It consists of a number of sources, storage ports and loads connected to it. Bidirectional power flow paths are also possible in this structure. Since MPC acts as a single power processing unit, a centralized power control system can be used which eases the control complexity [15]-[20].

Journal of Energy Engineering and Thermodynamics
ISSN: 2815-0945
Vol: 02, No. 05, Aug-Sep 2022
http://journal.hmjournals.com/index.php/JEET
DOI: https://doi.org/10.55529/jeet.25.1.19

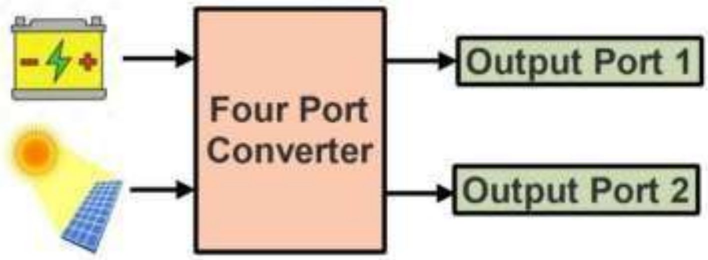

Fig.1 Structure of Four-port converter

The four-port converter integrates two inputs and two outputs. This topology is utilized for DC bus application and thus identification of ports for a simple four port application is as follows;

1. One of the ports at the primary side is chosen as a PV power source.
2. Another port at the primary side is chosen as a storage source (Battery).

The last two ports are the bipolar load port.

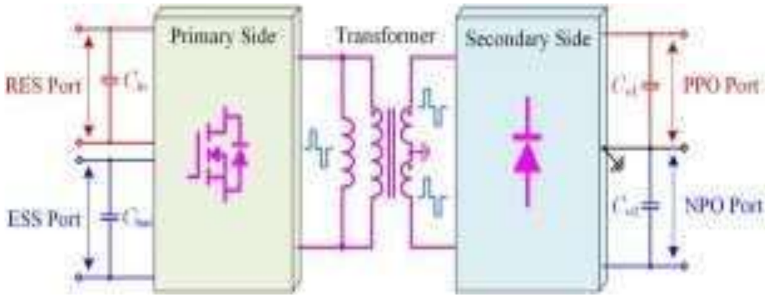

Fig.2 The proposed isolated four-port converter's basic design

In this paper, the Full Bridge Interleaving Bidirectional Buck Boost + Semi Active Rectifier (FB-IB3+SAR-BO) converter is designed and simulation study is carried out. The PV source and Battery storage system are the input source of the Four Port Converter (FPC). The performance of the converter is investigated for different solar intensities and battery voltages. The effect of Duty ratio is studied and optimum duty ratio for regulated output of 60 V is identified and the results are discussed.

Journal of Energy Engineering and Thermodynamics
ISSN: 2815-0945
Vol: 02, No. 05, Aug-Sep 2022
http://journal.hmjournals.com/index.php/JEET
DOI: https://doi.org/10.55529/jeet.25.1.19

Proposed Topology of Isolated Four Port Converter

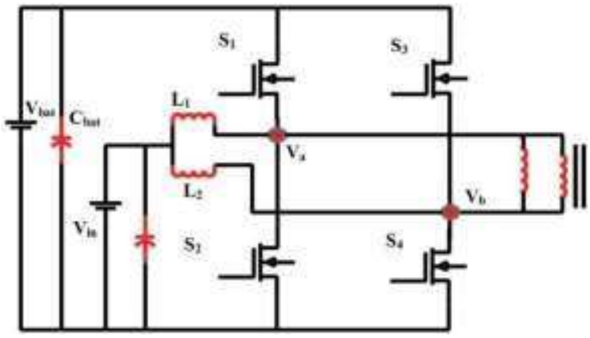

Fig. 3 Topology of the proposed Circuit (Primary Side)

In the primary side, Topology converter circuit is utilized to reverse the input potential of RES and ESS in the large frequency AC voltage being delivered to the Center-tapped transformer. It consists of Four switches S1 – S4 and two inputs such as PV power source and a Battery.

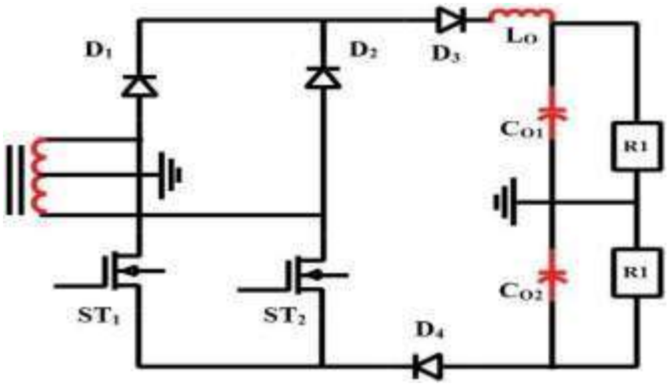

Fig. 4 Semi-Active Rectifier with Bipolar Outputs

The Secondary side of proposed converter, the topology is Semi-Active Rectifier (SAR-BO) is considered to rectify the high-frequency AC voltage into Bipolar DC output. It consists of two switches and four diodes D1 – D4 with Bipolar outputs.

Journal of Energy Engineering and Thermodynamics
ISSN: 2815-0945
Vol: 02, No. 05, Aug-Sep 2022
http://journal.hmjournals.com/index.php/JEET
DOI: https://doi.org/10.55529/jeet.25.1.19

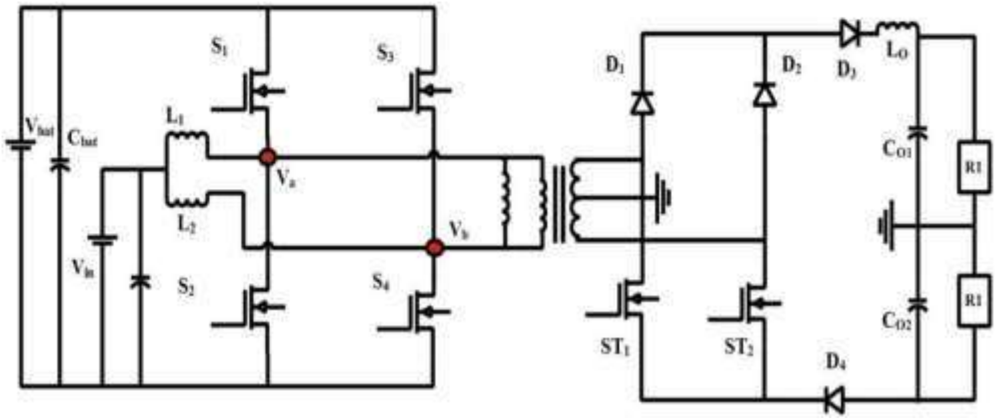

Fig. 5 Proposed converter complete circuit

Proposed Converter Description

Because of the extensive soft switching choice and limited count of semiconductors and magnetic elements, FB-IB3 and SAR-BO were chosen as the primary and secondary side circuits, respectively. The interweaving bi-directional buck/boost circuit with two inductors (L1 and L2) and four switches S1–S4 makes up the primary side. S1 and S2 (S3 and S4) have complementary driving signals. The currents of inductors L1 and L2 are iL1 and iL2, correspondingly, and the current of the RES is Iin. The two switch legs are powered in an interleaved fashion with a 180° phase shift angle, which helps to decrease the RES port's input current ripple. The range of D is controlled by the voltages of the RES and ESS ports, and the duty cycle of S1 is set as D. The primary and secondary sides of the transformer have a turn ratio of 1:n:n. ST1 and ST2 are driven complementarily on the secondary side of the converter with a fixed duty cycle of 0.5. Depending on the primary side winding current ip, the proposed circuit can function in continuous current mode (CCM) or discontinuous current mode (DCM). The operation of the converter under the CCM is explored and analyzed in depth in this article. In this scenario, one switching period contains 14 operation stages. Only

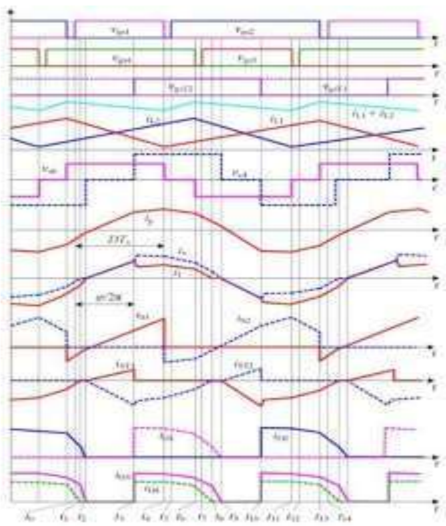

Fig. 6 Steady state waveforms of the proposed converter

Journal of Energy Engineering and Thermodynamics
ISSN: 2815-0945
Vol: 02, No. 05, Aug-Sep 2022
http://journal.hmjournals.com/index.php/JEET
DOI: https://doi.org/10.55529/jeet.25.1.19

seven operating steps in a half switching time are shown due to circuit symmetry. The essential waveforms are depicted, as well as the comparable circuits in each switching level. The following is a detailed operational examination of each mode. vgs1–vgs4 are the driving signals of switches S1–S4, where S1 and S2 (S3 and S4) have complimentary driving signals and the driving signals of S1 and S3 have a 180° phase shift. Furthermore, vgsT1–vgsT2 are the driving signals for the switches ST1–ST2, which are operated complementarily with a set duty cycle of 0.5. Vab and vcd, correspondingly, are the potentials amongst the center of the primary and secondary side rectifier legs. The primary side winding Np, secondary side winding Ns, and third side winding Nt, respectively, have currents of ip, is, and it. The currents of diodes D1–D4 are denoted by iD1–iD4.

Operation Modes

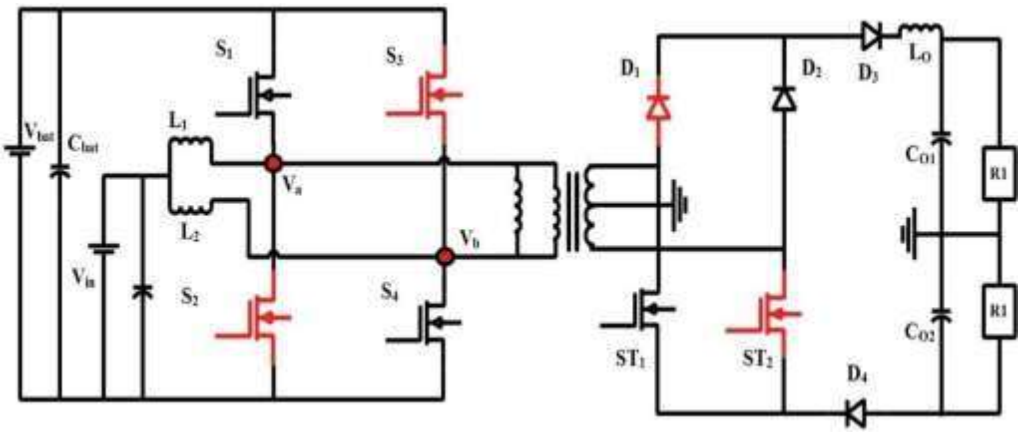

Fig. 7 (a) Operation of Mode 1

In Fig 7(A), S4 and ST1 are turned on before t0, at the interval between S2 and S1. Through S4 and S1's body diode, the primary side winding current ip passes, the inductor L1 is linearly de-energized, iL1 is linearly decreasing. With the voltage Vin, the inductor L2 is linearly activated, and iL2 is linearly growing. The secondary side windings Ns and Nt send power to the NPO and PPO ports via ST1 and D4, D2, and D3, while the primary side winding current ip is calculated as ip (t) = ip (t0) + (Vbat + Vo1/n) (t-t0)/Lk.

Journal of Energy Engineering and Thermodynamics
ISSN: 2815-0945
Vol: 02, No. 05, Aug-Sep 2022
http://journal.hmjournals.com/index.php/JEET
DOI: https://doi.org/10.55529/jeet.25.1.19

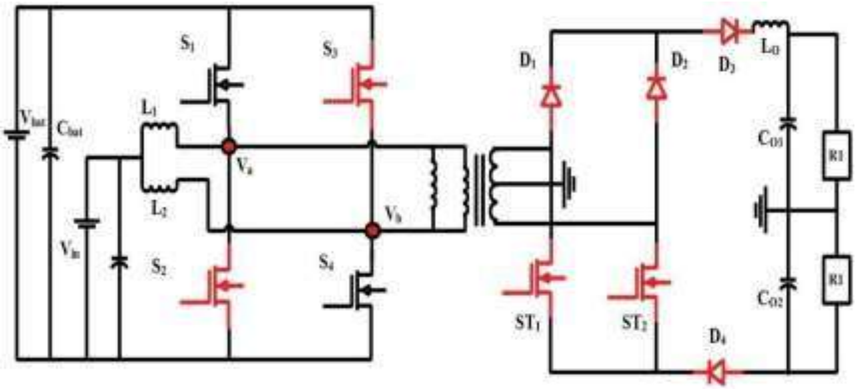

Fig. 7(b) Operation of Mode 2

In Fig 7(B), The PPO and NPO ports load currents meet Io1 > Io2, and the diode currents meet iD3 > iD4. The diode current iD4 and the secondary side winding Ns currents are both reduced to zero at time t1. In this stage, iL1 and iL2 are the same as in the previous one. This stage will come to a close at t2 when iD2 and iD3 reach zero.

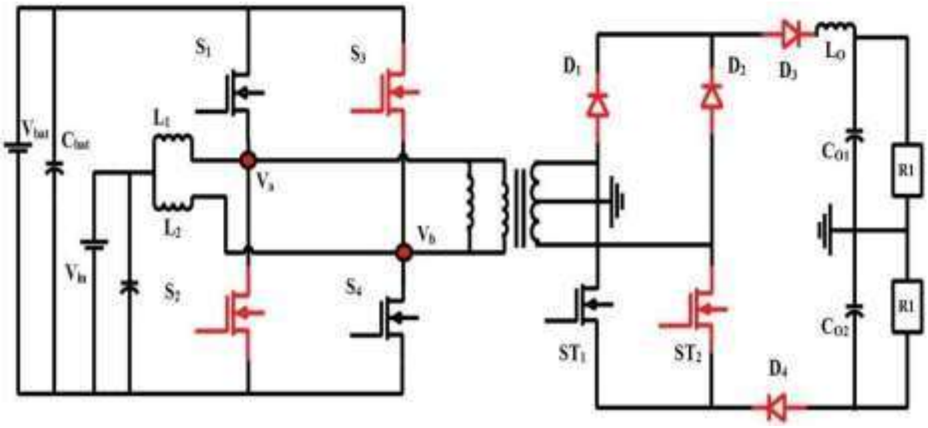

Fig. 7(c) Operation of Mode 3

In Fig 7(C), The secondary side winding current is freewheeling at this point, just passing through ST1 and the ST2 body diode, and no energy is supplied from the secondary side to the bipolar load. ip (t) = ip (t2) + Vbat (t-t2)/Lk can be written as ip (t) = ip (t2) + Vbat (t-t2)/Lk at this stage.

Journal of Energy Engineering and Thermodynamics
ISSN: 2815-0945
Vol: 02, No. 05, Aug-Sep 2022
http://journal.hmjournals.com/index.php/JEET
DOI: https://doi.org/10.55529/jeet.25.1.19

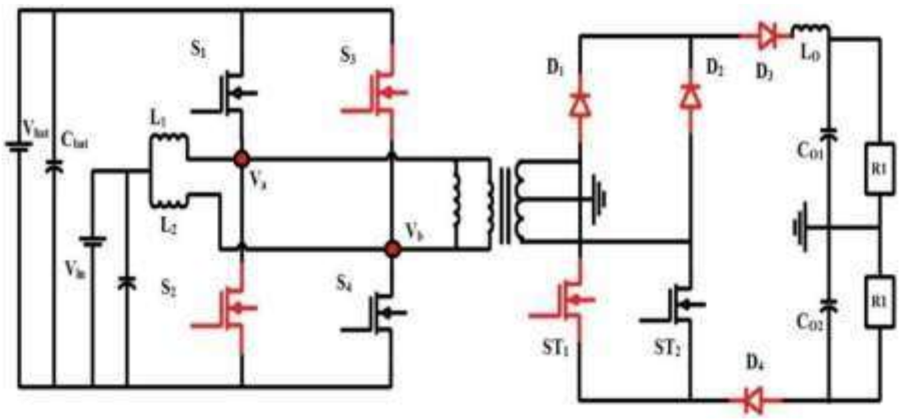

Fig. 7(d) Operation of Mode 4

In Fig 7(D), ST1 is swithed off and ST2 is switched on at time t3. Through D1 and D3, ST2 and D4, the secondary side windings Ns and Nt deliver power to the PPO and NPO ports, respectively. Vbat and Vo1 + Vo2 are the primary potential vab and secondary potential vcd, respectively.

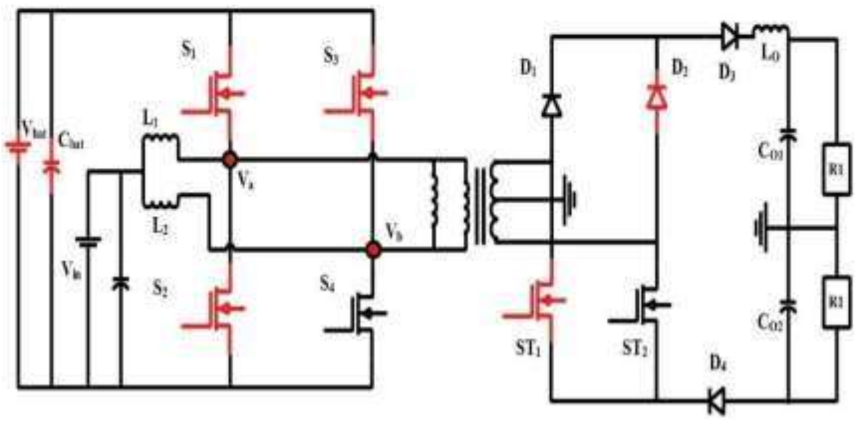

Fig. 7(e) Operation of Mode 5

In Fig 7(E), S4 is turned off at t4. With the voltage Vin, the inductors L2 are linearly powered, and iL2 remains to rise linearly. With the voltage Vin, the inductors L1 begin to be linearly powered, and iL1 begins to increase linearly. Through D1 and D3, ST2 and D4, the secondary windings Ns and Nt deliver power to the ports, correspondingly.

Journal of Energy Engineering and Thermodynamics
ISSN: 2815-0945
Vol: 02, No. 05, Aug-Sep 2022
http://journal.hmjournals.com/index.php/JEET
DOI: https://doi.org/10.55529/jeet.25.1.19

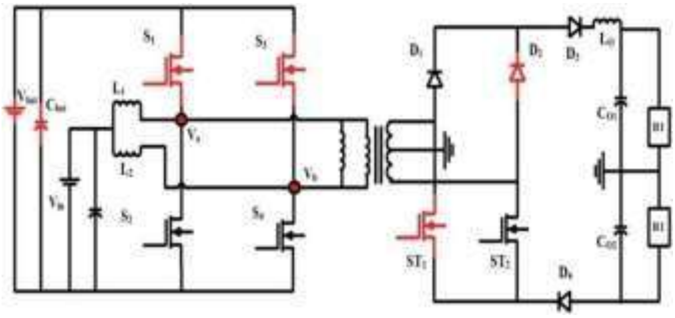

Fig. 7(f) Operation of Mode 6

In Fig 7(F), S2 is switched ON, at t5. The proposed circuit functions similar as 4th phase of operation.

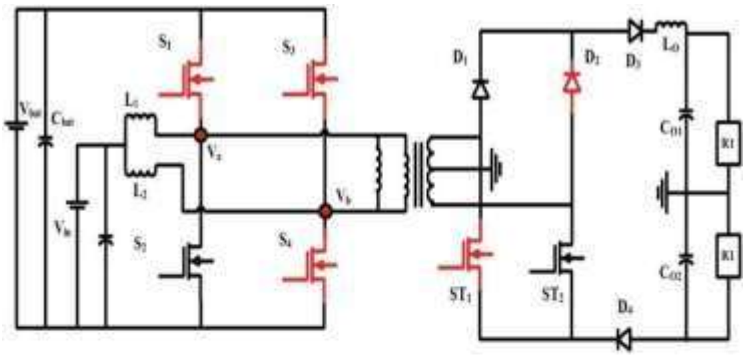

Fig. 7(g) Operation of Mode 7

In Fig 7(G), S4 is turned off at t6. Through D1 and D3, D4 and ST2, the secondary windings deliver power to the ports.

Specification of Proposed Converter

Table1: Specification of the converter

Parameter	**Value**	**Parameter**	**Value**
Output voltage (V_0)	±60v	Turn ratio n	n=0.9
PV voltage (V_{in})	30V	Magnetic Inductor L_m	120µH
PV current (I_{in})	0-10A	Leakage Inductor L_k	7µH
Inductor L_1 and L_2	85μH	Battery voltage	96V
Capacitors C_{bat} and C_{in}	220µF/100v	Switching frequency	100Khz
Capacitors C_{o1} and C_{o2}	330µF/150V	Diodes D_1 ~ D_2	STPS401120CT

Journal of Energy Engineering and Thermodynamics
ISSN: 2815-0945
Vol: 02, No. 05, Aug-Sep 2022
http://journal.hmjournals.com/index.php/JEET
DOI: https://doi.org/10.55529/jeet.25.1.19

2. SIMULATION RESULTS AND DISCUSSION

The simulation results of the FB-IB3 and SAR-BO proposed converter are discussed. The peak power of the panel at the standard conditions of temperature 25 ºC and intensity 1000 W/m2 is 250 Watts. Fig 8 (a) The I-V and (b)V-P characteristics of the panel are presented.

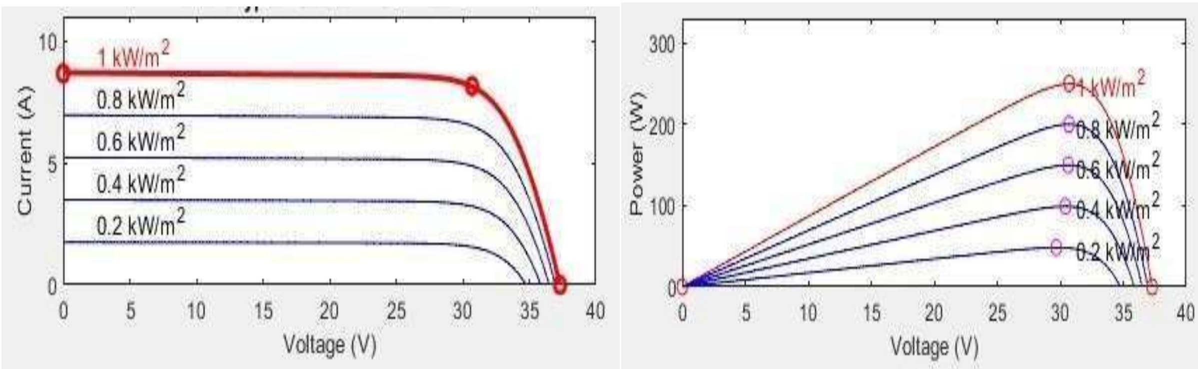

Fig. 8 VI and PV Characteristics of the Solar Panel

Battery charging and discharging
Battery = Lead acid Battery
Nominal voltage = 96 Volts
Battery rated capacity = 100 Ah
Initial State of Charge = 80

Simulation Results at rated condition and the waveforms
Intensity = 1000 W/m2
Battery voltage = 96Volts
Rated PV voltage VPV = 30 V
Rated PV current IPV = 0-10 A
Rated Load voltage V0 = 60 V
Rated Load current I0 = 12 V

Journal of Energy Engineering and Thermodynamics
ISSN: 2815-0945
Vol: 02, No. 05, Aug-Sep 2022
http://journal.hmjournals.com/index.php/JEET
DOI: https://doi.org/10.55529/jeet.25.1.19

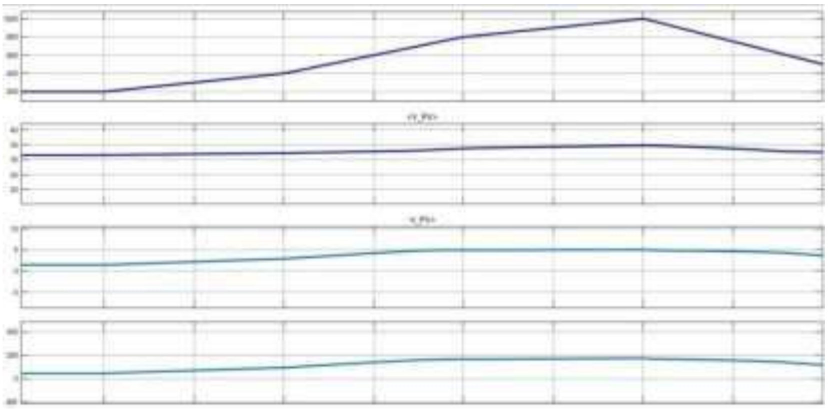

Fig. 10 Varying Solar intensities at duty ratio 0.5 with solar output

The following figures are the simulation study of Gate pulse for switches (S1-S4), ST1 and ST2 at rated condition

Fig. 11 Gate pulse for Switch S1 and S2 for 0.3 duty ratio

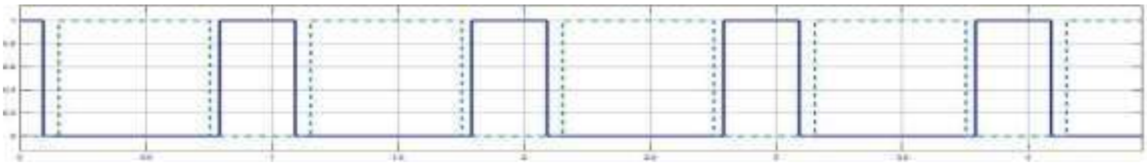

Fig. 12 Gate pulse for Switch S3 and S4 for 0.3 duty ratio

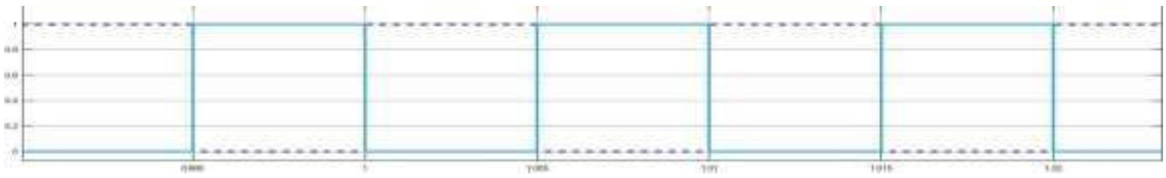

Fig. 13 Gate pulse for Switch ST1 and ST2 for 0.5 duty ratio

The following Fig 14 (a)-(h) are the simulation study of intermediate of the proposed circuit at rated condition

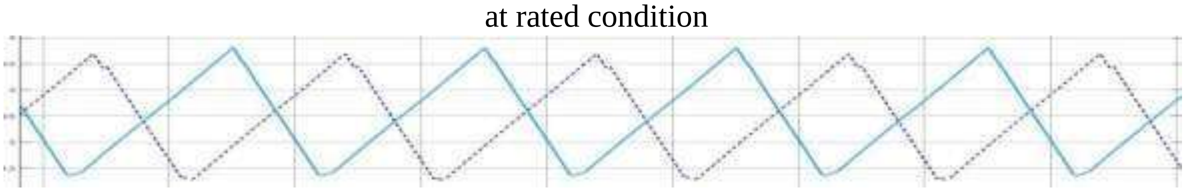

Fig. 14(a) The current of inductors L1 (il1) and L2 (il2),il1 = 3.6 A, il2 = 3.8 A

Journal of Energy Engineering and Thermodynamics
ISSN: 2815-0945
Vol: 02, No. 05, Aug-Sep 2022
http://journal.hmjournals.com/index.php/JEET
DOI: https://doi.org/10.55529/jeet.25.1.19

Fig. 14(b) The primary voltage Vab = 98 V, and the secondary side voltage Vcd = 140 V

Fig. 14(c) The current in the primary side circuit is ip = 21 A

Fig. 14(d) The current in the secondary side circuit is is it = 21 A, both is it synchronizes.

Fig. 14(e) The current through the switches S1 and S2 is1 = 22 A, is2 = 20 A

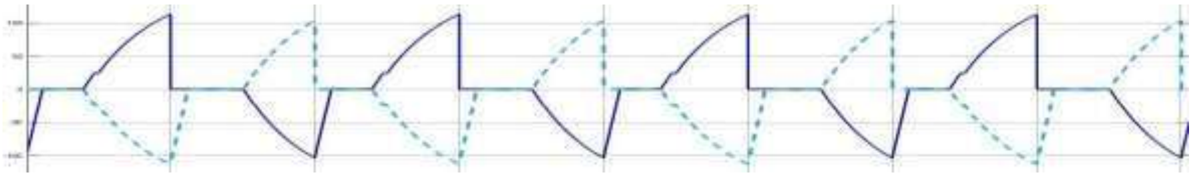

Fig. 14(f) The current through the switches ST1 and ST2 ist1 = 100 A, ist2 = 100 A

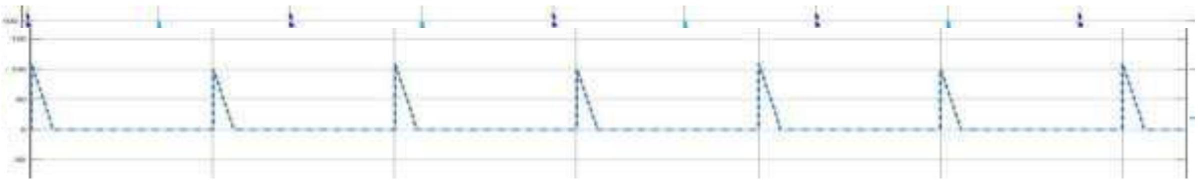

Fig. 14(g) The current through the Diodes D1 and D2 id1 = 102 A, id2 = 100 A
Fig. 14(h) The current through the Diodes D3 and D4 id3 = 100 A, id4 = 100 A, both id3 id4 synchronizes.

Journal of Energy Engineering and Thermodynamics
ISSN: 2815-0945
Vol: 02, No. 05, Aug-Sep 2022
http://journal.hmjournals.com/index.php/JEET
DOI: https://doi.org/10.55529/jeet.25.1.19

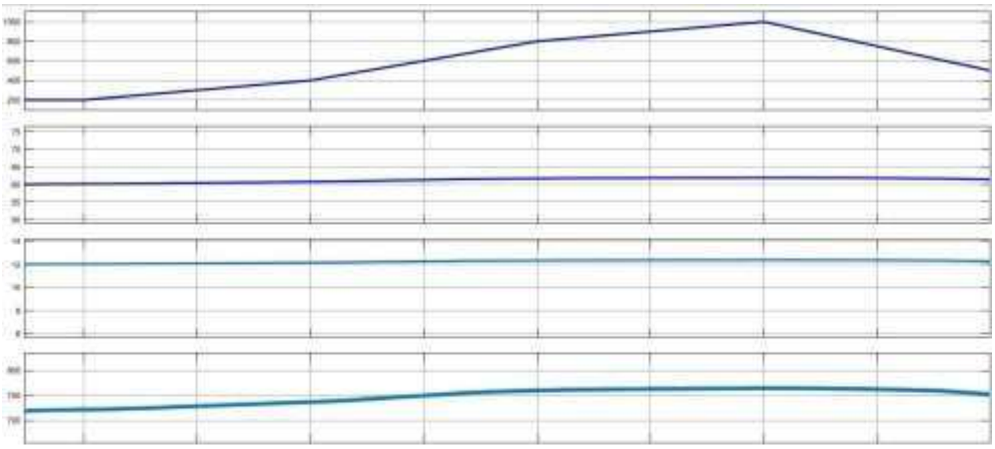

Fig. 15 varying solar intensities with bipolar outputs at rated duty ratio 0.5

Simulation results for different Battery voltage

Solar panel output for various Intensities

The solar PV panel output such as PV voltage, PV current, PV power for fixed duty ratio of 0.5 are plotted against various Intensities for different battery voltage such as 96 v, 70v, 60 v, 40 v, 20 v, 0 v.

Intensity vs PV Voltage V_{PV}

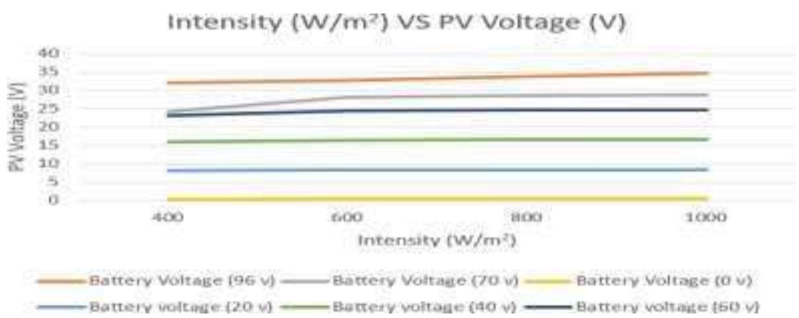

16 (a)

Intensity vs PV Current I_{PV}

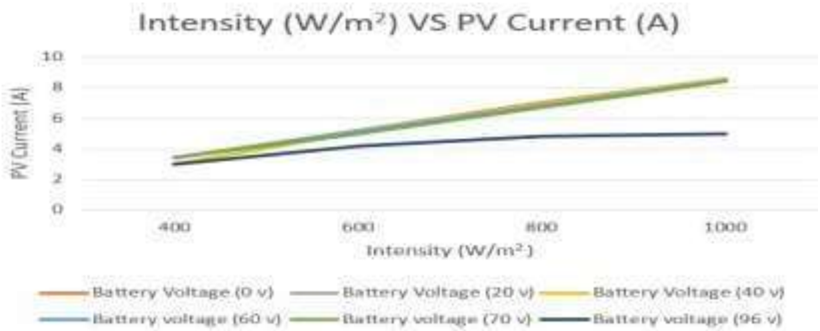

16 (b)

Journal of Energy Engineering and Thermodynamics
ISSN: 2815-0945
Vol: 02, No. 05, Aug-Sep 2022
http://journal.hmjournals.com/index.php/JEET
DOI: https://doi.org/10.55529/jeet.25.1.19

Intensity vs PV Power P_{PV}

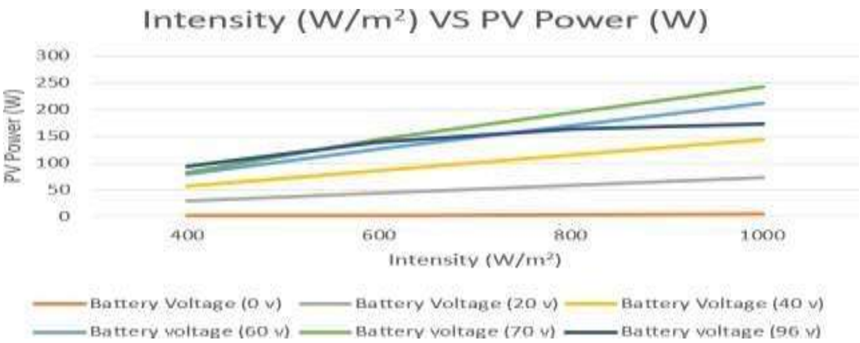

16 (c)

Fig. 16 Solar panel output (a) Voltage VPV (b) Current IPV (c) Power PPV

Bipolar output for various Intensities

The obtained Bipolar Output such as Load voltage, Load current, Load power for fixed duty ratio of 0.5 are plotted against various intensities for different battery voltage such as 96 v, 70v, 60 v, 40 v, 20 v, 0 v.

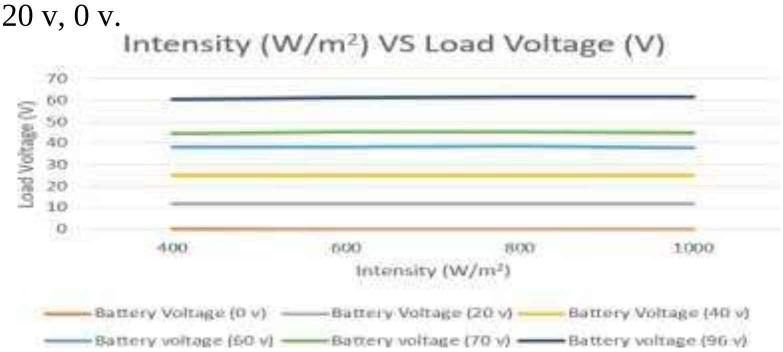

17 a) Intensity vs Load Voltage

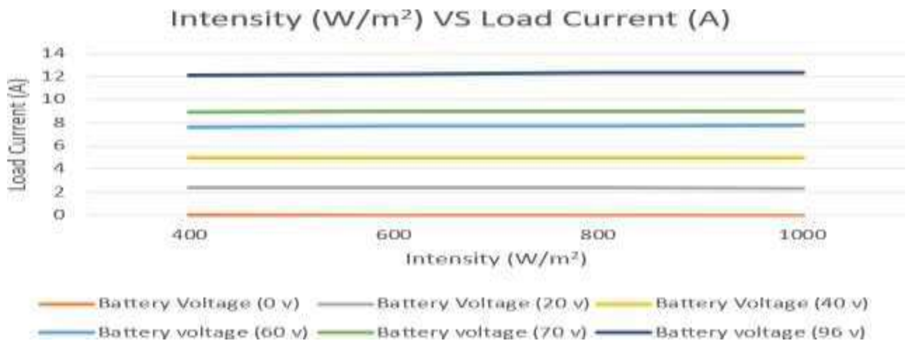

17 b) Intensity vs Load Current

Journal of Energy Engineering and Thermodynamics
ISSN: 2815-0945
Vol: 02, No. 05, Aug-Sep 2022
http://journal.hmjournals.com/index.php/JEET
DOI: https://doi.org/10.55529/jeet.25.1.19

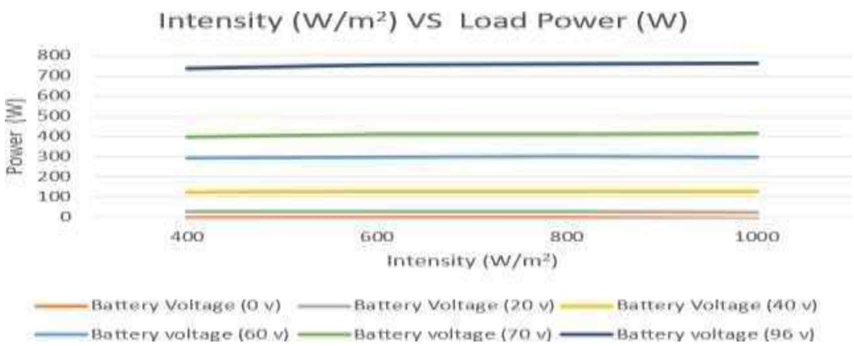

17 c) Intensity vs Load Power

Fig 17 Bipolar output (a) Output Voltage V0, (b) Output Current I0, (c) Output Power P0

Effects of Duty Ratio at intensity 1000 W/m2

For intensity 1000, plotting duty ratio vs solar panel output and bipolar output.

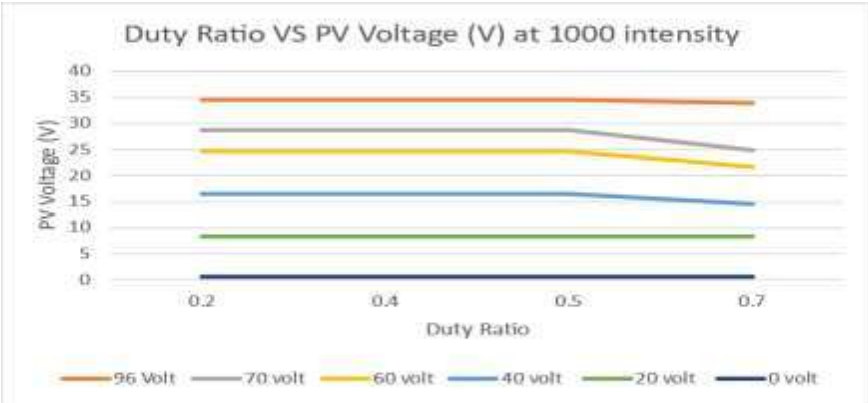

18 a) Duty Ratio vs PV voltage

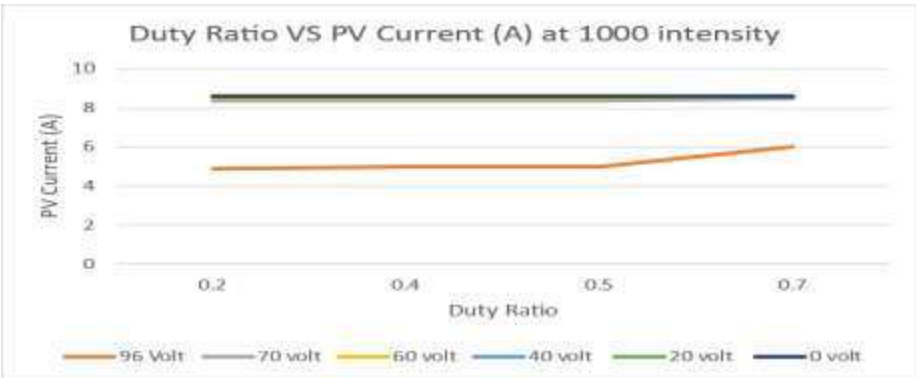

18 b) Duty Ratio vs PV current

Journal of Energy Engineering and Thermodynamics
ISSN: 2815-0945
Vol: 02, No. 05, Aug-Sep 2022
http://journal.hmjournals.com/index.php/JEET
DOI: https://doi.org/10.55529/jeet.25.1.19

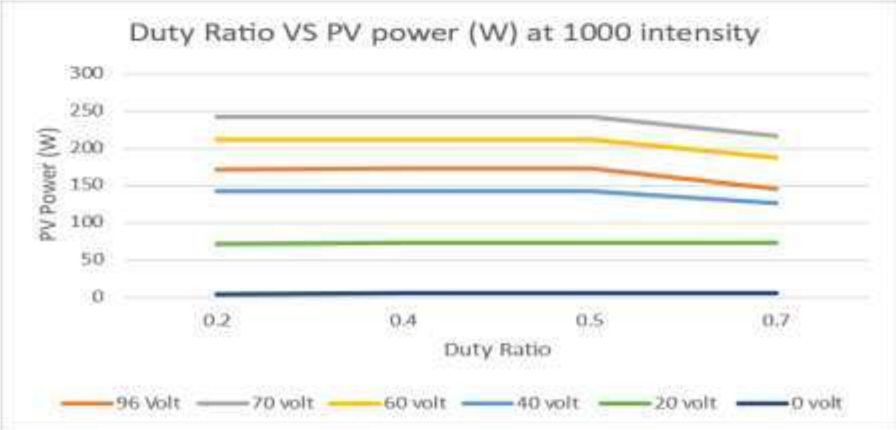

18 c) Duty Ratio vs PV power

Fig. 18 At 1000 W/m2 Duty ratio vs solar output, (a)PV voltage VPV, (b) PV current IPV, (c)PV power PPV.

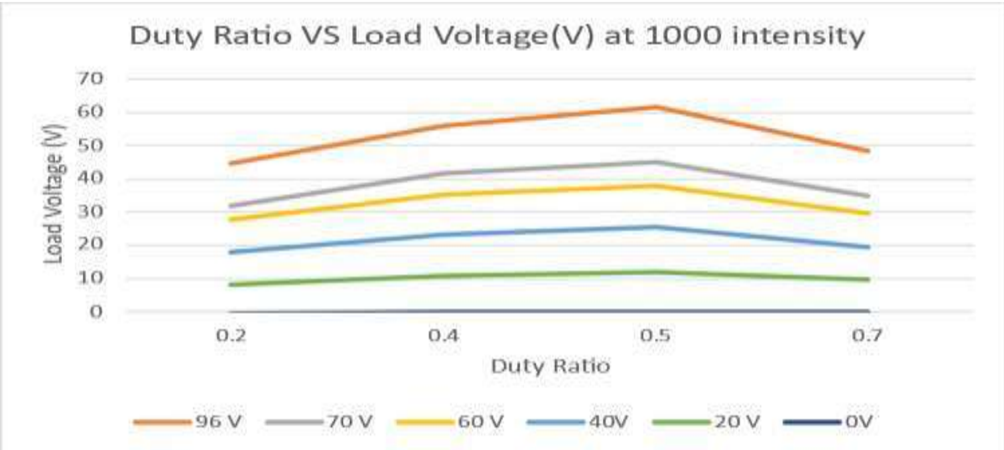

19 a) Duty Ratio vs Load voltage

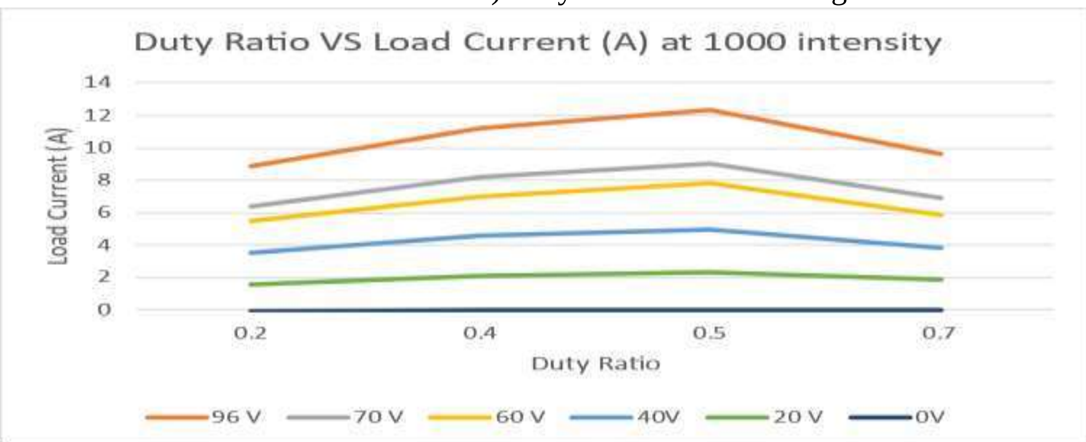

19 b) Duty Ratio vs Load current

Journal of Energy Engineering and Thermodynamics
ISSN: 2815-0945
Vol: 02, No. 05, Aug-Sep 2022
http://journal.hmjournals.com/index.php/JEET
DOI: https://doi.org/10.55529/jeet.25.1.19

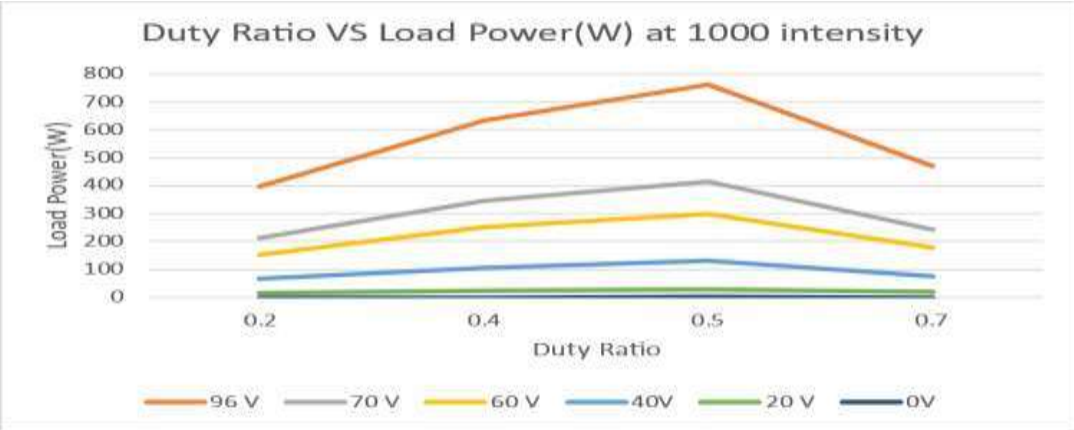

19 c) Duty Ratio vs Load power

Fig. 19 At 1000 W/m2 Duty ratio vs bipolar output, (a) Load voltage V0, (b) Load current I0, (c) Load power P0

From the Solar PV panel output such as PV voltage, PV current, PV power, for various duty ratio the PV voltage remains constant for each battery voltage. The PV power increases for every Battery voltage.

From the Bipolar output, it can be seen that load voltage, load current and load power at all intensities reaches Maximum at 0.5 Duty ratio, the load voltage 61.7 V, load current 12.3 A, and the load power 761 W for 0.5 duty ratio

3. CONCLUSION

In this paper, a 4-port converter built on center tapped winding for bi-polar DC bus usages is studied through simulation. When compared to the traditional converter, multi-port converter (MPC) acts as a single power converter and it connects a number of elements at different port, a four-port converter (FPC) said to occupied its place viewing diversified merits. with this viewpoint, the proposed topology is considered in this project. Then over-all assembly of isolated 4-port converter circuit output is explained in detailed.

The essence of the topology of the FB-IB3 and SAR-BO and the circuit diagram of the proposed converter are presented. The simulation results pertaining to the PV panel, the I-V and P-V characteristics. The battery charging and discharging characteristics has been discussed. The simulation results at rated condition and the steady-state waveforms are analyzed and discussed. The simulation results of Solar PV panel output, Bipolar output is plotted against various intensities at different battery voltage are obtained and also the Effects of duty ratio at various intensities are obtained and it has been observed that Bipolar output reaches maximum at 0.5 Duty ratio. The battery charging and discharging at different duty ratio has been observed and all the simulation results are verified and discussed.

4. REFERENCES

1. H. Moradisizkoohi, N. Elsayad, and O. A. Mohammed, “A family of three-port three-

level converter based on asymmetrical bidirectional half-bridge topology for fuel cell electric vehicle applications," IEEE Trans. Power Electron., vol. 34, no. 12, pp. 11706–11724, Dec. 2019.
2. J. Zhang et al., "A three-port LLC resonant dc/dc converter," IEEE J. Emerg. Sel. Topics Power Electron., vol. 7, no. 4, pp. 2513–2524, Dec. 2019.
3. O.Ellabban, H. Abu-Rub, and F. Blaabjerg, "Renewable energy resources: Current status, future prospects and their enabling technology," Renewable Sustain. Energy Rev., vol. 39, pp. 748–764, Nov. 2014.
4. G. Zhou, Q. Tian, M. Leng, X. Fan, and Q. Bi, "Energy management and control strategy for DC microgrid based on DMPPT technique," IET Power Electron., vol. 13, no. 4, pp. 658–668, Mar. 2020.
5. Jianwu Zeng, Senior Member, IEEE, Xia Du, Student Member, IEEE, Zhaoxia Yang, Student Member, IEEE "A Multiport Bidirectional DC-DC Converter for Hybrid Renewable Energy System Integration", 2021
6. M. Uno and K. Sugiyama, "Switched capacitor converter based multiport converter integrating bidirectional PWM and series-resonant converters for standalone photovoltaic systems," IEEE Trans. Power Electron., vol. 34, no. 2, pp. 1394–1406, Feb. 2019.
7. Majid Ghani Varzaneh, Amirhossein Rajaei , Member, IEEE, Mojtaba Forouzesh , Student Member, IEEE, Yam P. Siwakoti , Senior Member, IEEE, "A Single-Stage Multi-Port Buck-Boost Inverter", July 2021
8. Shashank Kurm, Student Member, IEEE, and Vivek Agarwal, IEEE "Dual Active Bridge Based Reduced Stage Multiport DC/AC Converter for PV-Battery Systems", April 2022
9. Masanori Ishigaki, Member, IEEE, Keisuke Ishikawa, Makoto Kusakabe, and Kosuke Tahara "Multi-port, Bi-directional Contactless Connector for the Interface of Modular Portable Battery System", 2020
10. Chatumal Perera, John Salmon, and gregory J. Kish (Senior Member, IEEE) "Multiport Converter With Enhanced Port Utilization Using Multitasking Dual Inverters", September 2021
11. Qingxin Tian, Guohua Zhou , Senior Member, IEEE, Lei Wang , Student Member, IEEE, Qiang Bi , Student Member, IEEE, and Minrui Leng "Symmetric Bipolar Output Full-Bridge Four-Port Converter With Phase-Shift Modulated Buck–Boost Voltage Balancer", august 2022
12. Qingxin Tian, Student Member, IEEE, Guohua Zhou, Senior Member, IEEE, Ruijun Liu, Xiaobing Zhang, Student Member, IEEE, Minrui Leng, Student Member, IEEE "Topology Synthesis of a Family of Integrated Three-Port Converters for Renewable Energy System Applications", 2020
13. Q. Tian, G. Zhou, R. Liu, X. Zhang, and M. Leng, "Topology synthesis of a family of integrated three-port converters for renewable energy system applications," IEEE Trans. Ind. Electron., vol. 68, no. 7, pp. 5833–5846, Jul. 2021
14. B. Li, Q. Fu, S. Mao, X. Zhao, and D. Xu, "DC/DC converter for bipolar LVDC system with integrated voltage balance capability," IEEE Trans. Power Electron., vol. 36, no. 5, pp. 5415–5424, May 2021.
15. G.Chen, Y. Liu, X. Qing, and F. Wang, "Synthesis of integrated multiport dc-dc converters with reduced switches," IEEE Trans. Ind. Electron., vol. 67, no. 6, pp. 4536–

4546, Jun. 2020.
16. T. Jalilzadeh, N. Rostami, E. Babaei, and S. H. Hosseini, “Multiport DC–DC converter with step-up capability and reduced voltage stress on switches/diodes,” IEEE Trans. Power Electron., vol. 35, no. 11, pp. 11902–11915, Nov. 2020.
17. J. Lee, Y. Cho, and J. Jung, “Single-stage voltage balancer with high frequency isolation for bipolar LVDC distribution system,” IEEE Trans. Ind. Electron., vol. 67, no. 5, pp. 3596–3606, May 2020.
18. J.-Y. Lee, H.-S. Kim, and J.-H. Jung, “Enhanced dual-active-bridge dc-dc converter for balancing bipolar voltage level of dc distribution system,” IEEE Trans. Ind. Electron., vol. 67, no. 12, pp. 10399–10409, Dec. 2020.
19. Q. Tian, G. Zhou, M. Leng, G. Xu, and X. Fan, “A non-isolated symmetric bipolar output four-port converter interfacing PV-battery system,” IEEE Trans. Power Electron., vol. 35, no. 11, pp. 11731–11744, Nov. 2020.
20. P. Prabhakaran and V. Agarwal, “Novel boost-SEPIC type interleaved dc-dc converter for mitigation of voltage imbalance in a low-voltage bipolar dc microgrid,” IEEE Trans. Ind. Electron., vol. 67, no. 8, pp. 6494–6504, Aug. 20.
21. S. M. Metev and V. P. Veiko, Laser Assisted Microtechnology, 2nd ed., R. M. Osgood, Jr., Ed. Berlin, Germany: Springer-Verlag, 1998.
22. J. Breckling, Ed., The Analysis of Directional Time Series: Applications to Wind Speed and Direction, ser. Lecture Notes in Statistics. Berlin, Germany: Springer, 1989, vol. 61.
23. S. Zhang, C. Zhu, J. K. O. Sin, and P. K. T. Mok, “A novel ultrathin elevated channel low-temperature poly-Si TFT,” IEEE Electron Device Lett., vol. 20, pp. 569–571, Nov. 1999.
24. M. Wegmuller, J. P. von der Weid, P. Oberson, and N. Gisin, “High resolution fiber distributed measurements with coherent OFDR,” in Proc. ECOC’00, 2000, paper 11.3.4, p. 109.
25. R. E. Sorace, V. S. Reinhardt, and S. A. Vaughn, “High-speed digital-to-RF converter,” U.S. Patent 5 668 842, Sept. 16, 1997.
26. (2002) The IEEE website. [Online]. Available: http://www.ieee.org/
27. M. Shell. (2002) IEEEtran homepage on CTAN. [Online]. Available: http://www.ctan.org/tex-archive/macros/latex/contrib/supported/IEEEtran/
28. FLEXChip Signal Processor (MC68175/D), Motorola, 1996.
29. “PDCA12-70 data sheet,” Opto Speed SA, Mezzovico, Switzerland.
30. Karnik, “Performance of TCP congestion control with rate feedback: TCP/ABR and rate adaptive TCP/IP,” M. Eng. thesis, Indian Institute of Science, Bangalore, India, Jan. 1999.
31. J. Padhye, V. Firoiu, and D. Towsley, “A stochastic model of TCP Reno congestion avoidance and control,” Univ. of Massachusetts, Amherst, MA, CMPSCI Tech. Rep. 99-02, 1999.
32. Wireless LAN Medium Access Control (MAC) and Physical Layer (PHY) Specification, IEEE Std. 802.11, 1997.